Chemotaxis in shear flow: similarity solutions of the steady-state chemoattractant and bacterial distributions

Journal:	*AIChE Journal*
Manuscript ID	AIChE-19-21320.R2
Wiley - Manuscript type:	Research Article
Date Submitted by the Author:	n/a
Complete List of Authors:	Shim, Suin; Princeton University, Mechanical and Aerospace Engineering Stone, Howard; Princeton University, Mechanical & Aerospace Engineering Ford, Roseanne; University of Virginia, Department of Chemical Engineering
Keywords:	Chemotaxis, Similarity solutions, Shear flow

Chemotaxis in shear flow: similarity solutions of the steady-state chemoattractant and bacterial distributions

Suin Shim[1], Howard A. Stone[1] and Roseanne M. Ford[2]

[1] Department of Mechanical and Aerospace Engineering, Princeton University, Princeton, NJ 08544, USA

[2] Department of Chemical Engineering, School of Engineering and Applied Science, University of Virginia, Charlottesville, Virginia 22904, USA

When chemotactic bacteria are exposed to a concentration gradient of chemoattractant while flowing along a channel, the bacteria accumulate at the interface between the chemoattractant source and bacterial suspension. Assuming that the interface is no-slip, we can apply the shear flow approximation near the no-slip boundary and solve for a steady-state convection-diffusion model for both chemoattractant and bacterial concentrations. We suggest similarity solutions for the two-dimensional problem and identify a critical length scale η_c for bacteria chemotaxis in a given concentration gradient. The analysis identifies three dimensionless groups representing, respectively, chemotactic sensitivity, the chemotaxis receptor constant, and the bacteria diffusion coefficient, which typically show coupled effects in experimental systems. We study the effect of the dimensionless groups separately and provide understanding of the system involving shear flow and chemotaxis.

I. Introduction

Oil-phase pollutants and other non-aqueous phase liquids (NAPL) that are trapped within the pore space of water-saturated soil create isolated sources that leach slowly into groundwater and nearby drinking water wells [1, 2]. Chemotactic bacteria, which are also able to degrade chemical contaminants, bias their migration towards the source [3], thereby increasing bacterial numbers in close proximity to the pollutant and ultimately increasing the rate of biodegradation [4, 5]. The geometrical conditions representative of the pore space and flow structure of groundwater can be demonstrated in microfluidic channels. Typically, the chemoattractant diffuses into the water in the direction transverse to the flow, so chemotaxis has been studied in the shear flow configurations both experimentally [6–12] and theoretically [13, 14].

As one motivation for the NAPL transport problem we consider a microfluidic device that was designed to capture some features of this environmental scenario [6]. The analysis reported here, in fact, applies generally to any shear flow, chemotactic configuration with modestly high Peclet number. In the experimental system of Wang et al. [6] a bacterial suspension (*Pseudomonas putida* F1) of fixed concentration flows past a $\ell = 50$-μm wide opening in a rectangular channel (height $h = 20$ μm by width $w = 2.5$ mm by length $L = 5$ cm) containing a trapped oil phase; see Figure 1(a,b). Chemoattractant (toluene) was dissolved in mineral oil at a volume ratio of 1:3. The high viscosity of mineral oil ($\mu_{\text{oil}} = 0.03$-0.14 Pa·s [6]) ensures that the oil phase does not penetrate into the PDMS (polydimethylsiloxane). Toluene is soluble in the aqueous phase and so a chemical concentration gradient is generated that attracts chemotactic bacteria toward the source. *P. putida* exhibit a run-and-reverse swimming pattern, which is similar to the run-and-tumble mechanism of *E. coli*, but with a bimodal turn angle distribution that favors forward and reverse directions in comparison to *E. coli* [15]. In the experiments described in [6], bac-

teria cells flow in the x direction and are exposed to chemoattractant that is diffusing in the transverse (y) direction from the oil-water interface. In the original experiments the steady-state distribution of bacteria was recorded for a range of mean flow speeds $\langle u \rangle$ = 6-120 μm/s.

In such experimental systems in a rectangular cross-section microfluidic channel, the velocity profile near the walls can be approximated as a shear flow (we can assume the no-slip boundary condition since $\mu_{\text{oil}} \gg \mu_{\text{water}}$). For $h \ll w$, the shear rate near the wall varies as $\langle u \rangle / h$, and if $h = O(\ell)$, the shear rate at the interface can be estimated as $\dot{\gamma} \approx \dfrac{\langle u \rangle}{\ell}$. Typical values of the Peclet number Pe in the experiments of [6] for characterizing transport in the x-y plane (Figure 1(b)) range from $Pe = \dfrac{\langle u \rangle \ell}{D_A} \approx \dfrac{\dot{\gamma} \ell^2}{D_A} \approx$ 0.35-7, where D_A is the diffusivity of the chemoattractant ($D_A \approx 8.6 \times 10^{-10}$ m^2/s) [7]. Higher Peclet numbers

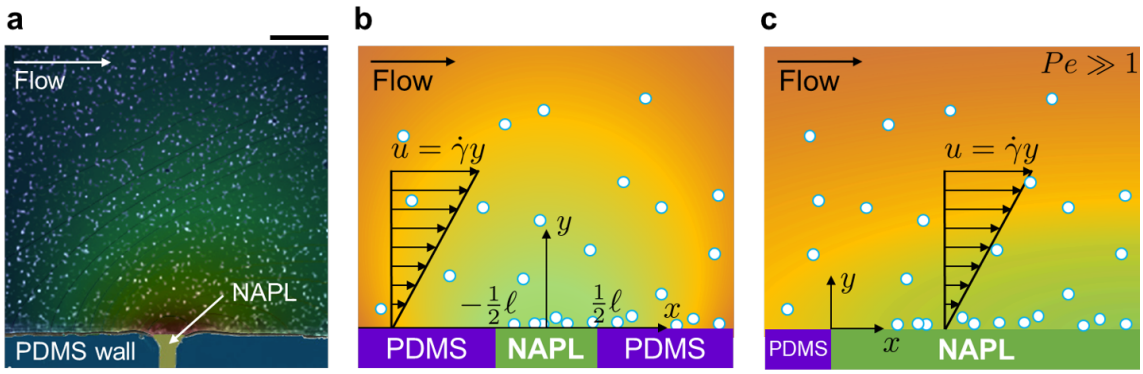

Figure 1: (a) Experimental image from Wang et al. [6]. The white dots in the background are bacterial cells. Scale bar is 100 μm. (b) Schematic drawing for arbitrary Peclet number of the flow near the chemoattractant window as an approximation to the shear flow near a surface. Bacterial suspension is indicated as white dots and the green and orange colors approximates the chemoattractant distribution. We solve for the chemoattractant and bacterial concentration in the aqueous phase. For the general problem statement, we consider the region that is larger than the typical length scale of the oil-water interface. (c) Schematic of the shear flow near the chemoattractant for the large Peclet number limit ($Pe \gg 1$). In this limit, we analyze the boundary region near the downstream part of the NAPL entrance and we shift the origin of the x axis.

are naturally generated with only modestly larger scales since $Pe \propto \ell^2$.

Here we consider a model problem with the shear flow approximation, motivated by the experimental system in Figure 1. We first set up the two-dimensional model problem (Figure 1(b)) in the aqueous phase, then analyze the limit where $Pe \gg 1$ (Figure 1(c)) so that the boundary layer approximation can be applied for the diffusion terms ($\frac{\partial^2}{\partial x^2} \ll \frac{\partial^2}{\partial y^2}$, where x and y are defined, respectively, as along and across the direction of the flow [16,17]). For the steady-state behavior of both chemoattractant and bacteria, we solve, respectively, convection-diffusion equations with the shear flow and chemotaxis velocity (see next section) and provide similarity solutions to understand the critical length scale beyond which the bacteria concentration is unperturbed from its input value. By defining and investigating the dimensionless groups that characterize the system, we better characterize the steady-state behavior of chemotactic bacteria under a shear flow. The analysis also suggests a more effective approach to evaluate transport parameters for bacterial chemotaxis.

II. Theory

1. Steady-state equations for chemoattractant and bacteria

Consider steady flow of a bacterial suspension in a rectangular channel as shown in Figure 1(b). From a small opening of width ℓ, the flow is exposed to a non-aqueous phase liquid (NAPL) e.g., toluene, which is a chemoattractant. The chemical dissolves in water and the concentration of bacteria is expected to increase near the window as the suspension flows downstream. With the shear flow approximation in a two-dimensional configuration, we can write the steady-state convection-diffusion equation for the concentration $c_A(x, y)$ of a chemoattractant in water as

$$\dot{\gamma} y \frac{\partial c_A}{\partial x} = D_A \left(\frac{\partial^2 c_A}{\partial x^2} + \frac{\partial^2 c_A}{\partial y^2} \right) , \tag{1}$$

where $\dot{\gamma}$ is the shear rate and D_A is the diffusion coefficient of the chemical. The corresponding boundary conditions are,

$$c_A \left(|x| < \frac{\ell}{2}, 0 \right) = c_{A0} \tag{2a}$$

$$\frac{\partial c_A}{\partial y} \left(|x| > \frac{\ell}{2}, 0 \right) = 0 \tag{2b}$$

$$c_A \to 0 \quad \text{for} \quad \left(x^2 + y^2 \right)^{\frac{1}{2}} \to \infty , \tag{2c}$$

where the first condition (2a) assumes that the oil-water interface is in equilibrium.

We can write an equation for the bacterial distribution using the chemotactic velocity $\boldsymbol{v}_B(x, y)$ for shallow gradients, which is appropriate for most laboratory experiments and natural systems, defined as

$$\boldsymbol{v}_B = \frac{\chi_0 K_c}{3(K_c + c_A)^2} \nabla c_A , \tag{3}$$

where χ_0 is the chemotactic sensitivity coefficient and K_c is the chemotaxis receptor constant [14]. The representative values for D_A, χ_0, K_c and c_{A0} from the experimental system in Wang *et al.* [6] are, respectively, $D_A = 8.6 \times 10^{-10}$ m^2/s, $\chi_0 = 5.0 \times 10^{-10}$ m^2/s, $K_c = 1$ mM and $c_{A0} = 1.4$ mM. For D_A we use the the diffusion coefficient of toluene in water. We note that in such system we can define a chemical Peclet number $Pe_c = \dfrac{u_b \ell_b}{D_A}$, which measures the effect of bacterial swimming on the transport of chemicals (note that this is different from $Pe = \dfrac{\dot{\gamma} \ell^2}{D_A}$, which measures the relative advection due to the shear flow). u_b and ℓ_b are, respectively, the typical swimming speed (≈ 44 μm/s for *P. putida* [15]) and the length scale of the bacteria. For small molecules like toluene, the diffusion coefficient gives the value of $Pe_c \approx 10^{-2} \ll 1$ [18], and thus any convective mixing associated with

bacterial swimming is negligible compared to diffusion. Therefore, our analysis neglects any contributions from biomixing.

The steady-state convection-diffusion equation and the boundary conditions for bacteria are

$$\frac{\partial}{\partial x}\left(\dot{\gamma} y c_B + v_{Bx} c_B\right) + \frac{\partial}{\partial y}(v_{By} c_B) = D_B \left(\frac{\partial^2 c_B}{\partial x^2} + \frac{\partial^2 c_B}{\partial y^2} \right) , \tag{4a}$$

$$c_B \to c_{B0} \quad \text{for} \quad \left(x^2 + y^2\right)^{\frac{1}{2}} \to \infty \tag{4b}$$

$$v_{By} c_B|_{y=0} - D_B \frac{\partial c_B}{\partial y}\Big|_{y=0} = 0 \quad \text{for all } x \, , \tag{4c}$$

where $D_B = 3.2 \times 10^{-10}$ m^2/s is a representative value from the experimental system [6]. We note that the parameter value for bacterial diffusion is based on cell motility in a bulk aqueous phase. As bacteria encounter a boundary and under conditions of shear flow the swimming patterns of individual cells may be altered, which can impact the diffusion coefficient of the population. However, the magnitude of these effects appear to be second-order with respect to the order of magnitude analysis that we present in the paper. In fact, Molaei and Sheng [19] suggest that a shear field near the surface tends to offset the tumble suppression reported by Molaei *et al.* [20] for *E. coli* bacteria and the dispersion coefficient in the bulk phase is recovered as the shear rate approaches 30 s^{-1}. At a shear rate of 3 s^{-1} the reported mean run time (inverse of tumble frequency) decreased by only 15 % relative to that measured in the bulk fluid. Furthermore, we expect the run-and-reverse swimming pattern of *P. putida* to be less impacted by tumble suppression near the surface than the run-and-tumble pattern of *E. coli*. The final boundary condition (4c) reflects a balance of diffusion and convection (equation (3)) as there is no flux of bacteria through the lower boundary. In some cases, bacteria in shear flow near surfaces tend to swim upstream along the surface [21, 22] though this is an effect we neglect below because our interest is on transport of bacteria from the bulk fluid to the interface rather than over the interface.

2. Similarity solutions for $Pe \gg 1$ case

A. The chemoattractant

Here we consider the limit $Pe = \dfrac{\dot{\gamma}\ell^2}{D_A} \gg 1$. As is well-known [23], in this limit we can apply the boundary-layer approximation so that $\dfrac{\partial^2}{\partial y^2} \gg \dfrac{\partial^2}{\partial x^2}$ in the diffusion term in (1). Therefore, the steady-state equation for a non-reacting chemoattractant can be reduced to

$$\dot{\gamma} y \frac{\partial c_A}{\partial x} = D_A \frac{\partial^2 c_A}{\partial y^2} \ , \tag{5}$$

which allows us to describe the chemoattractant distribution in the neighborhood of the interface. Then the appropriate boundary conditions corresponding to 2(a-c) are

$$c_A(0, y) = 0, \quad c_A(x, 0) = c_{A0}, \quad \text{and} \quad c_A(x, y \to \infty) = 0 \ . \tag{6}$$

We can nondimensionalize the equation by defining

$$\bar{c}_A = \frac{c_A}{c_{A0}} \ , \qquad X = \frac{x}{\sqrt{D_A/\dot{\gamma}}} \ , \quad Y = \frac{y}{\sqrt{D_A/\dot{\gamma}}} \ . \tag{7}$$

The nondimensional equation and boundary conditions are

$$Y \frac{\partial \bar{c}_A}{\partial X} = \frac{\partial^2 \bar{c}_A}{\partial Y^2} \quad \text{with} \quad \bar{c}_A(0, Y) = 0, \quad \bar{c}_A(X, 0) = 1, \quad \text{and} \quad \bar{c}_A(X, Y \to \infty) = 0 \ . \tag{8}$$

Considering the structure of the equation, which is known as the Lévêque problem in chemical engineering, we can define a similarity variable $\eta = \frac{Y}{(3X)^{\frac{1}{3}}}$ and find a similarity solution $C_A(\eta) = \bar{c}_A(X, Y)$ [23, 24]. Equation (8) becomes

$$-\eta^2 \frac{dC_A}{d\eta} = \frac{d^2 C_A}{d\eta^2} \quad \text{and} \quad C_A(0) = 1 \text{ and } C_A(\infty) = 0 \ , \tag{9}$$

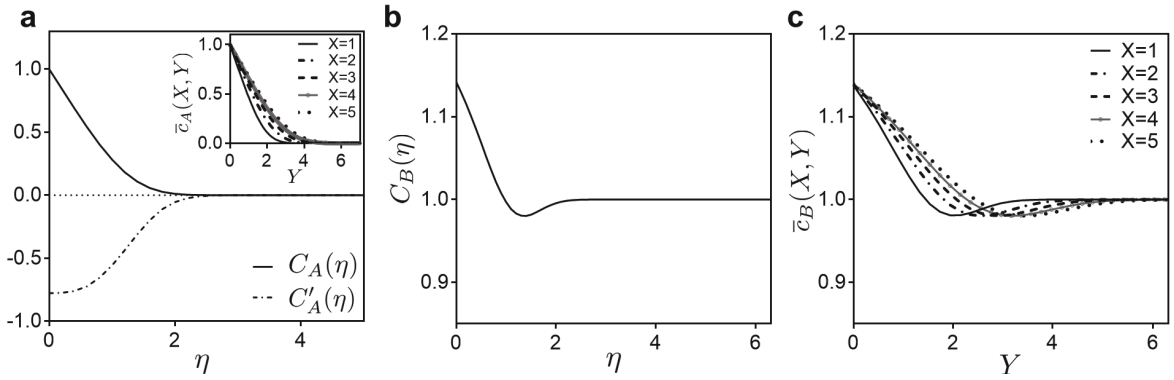

Figure 2: (a) $C_A(\eta)$ and C'_A plotted versus η. Inset: $\bar{c}_A$ plotted versus Y for different X values. (b) $C_B(\eta)$ plotted versus η. (c) $\bar{c}_B$ plotted versus Y for different X values. $\alpha = 0.6,\ \beta = 1.4,$ and $\delta = 0.35$. Note that in (b) and (c) we have magnified the vertical scale, which is near $\bar{c}_B(X,Y) \approx 1$.

and therefore we obtain the solution

$$C_A(\eta) = \frac{\Gamma\left(\frac{1}{3}, \frac{\eta^3}{3}\right)}{\Gamma\left(\frac{1}{3}\right)} \ . \tag{10}$$

where $\Gamma(\cdot)$ is the Gamma function and $\Gamma(\cdot,\cdot)$ is the incomplete Gamma function, i.e. $\Gamma\left(\frac{1}{3}, \frac{\eta^3}{3}\right) = \int_{\frac{\eta^3}{3}}^{\infty} t^{-\frac{2}{3}} e^{-t} \mathrm{dt}$. We note that within these approximations the boundary layer scale is $y/\ell \propto Pe^{-\frac{1}{3}} \ll 1$, which is evident from the structure of equation (5).

Results for $C_A(\eta)$ and $\frac{dC_A}{d\eta}$ are plotted versus η in Figure 2(a). Also, solutions obtained from equation (8) are plotted versus Y for different values of X (Figure 2(a) inset). The results from this well-known problem highlight the region near the boundary where chemoattractant is localized. The chemoattractant gradient directs bacterial motion, which we study in the next section.

B. Chemotaxis of bacteria

Next we consider the bacterial distribution in the field of the chemoattractant. The bacteria enter at concentration c_{B0}, and we assume that the initial bacterial concentration c_{B0} is small so that the motion of the individual bacterial cell does not perturb the macroscopic flow structure. With the assumption, we can develop our model to consider the distribution of bacteria under the influence of shear flow and chemotaxis. We anticipate that the effective bacterial diffusivity $D_B \leq D_A$ so that a typical bacterial Peclet number $Pe_B = \dfrac{\dot{\gamma}\ell^2}{D_B}$ is also large. It has been well studied that the bacteria concentration field is affected by a chemical gradient and one model for the migrating speed of the bacterial population is given by (3).

We then assume that for $\mathrm{Pe}_B \gg 1$ the x-directed contribution from (3) is small compared to the typical convective speed $\dot{\gamma}y$, hence for chemotaxis we retain only the y-component of velocity

$$v_{By} = \frac{\chi_0 K_c}{3(K_c + c_A)^2} \frac{\partial c_A}{\partial y} \ . \tag{11}$$

A simple scaling argument provides

$$\frac{v_{Bx}}{\dot{\gamma}y} \approx \frac{\chi_0 K_c}{(K_c + c_{A0})^2} \frac{c_{A0}}{\dot{\gamma}y^2} \approx \frac{\chi_0}{\dot{\gamma}y^2} \approx \frac{\chi_0}{D_A} Pe^{-\frac{1}{3}} \ll 1 \ , \tag{12}$$

suggesting that this approximation is valid for large Peclet numbers.

Now we can write the steady-state convection-diffusion equation for the bacterial concentration c_B,

$$\dot{\gamma}y \frac{\partial c_B}{\partial x} + \frac{\partial}{\partial y}(v_{By} c_B) = D_B \frac{\partial^2 c_B}{\partial y^2} \ , \tag{13}$$

with the boundary conditions $c_B(x \to 0, y) = c_B(x, \infty) = c_{B0}$ and at $y = 0$ (the oil-water interface) $v_{By} c_B - D_B \frac{\partial c_B}{\partial y} = 0$. Rewriting equation (13) with the expression (11), we have

$$\dot{\gamma} y \frac{\partial c_B}{\partial x} + \frac{\chi_0 K_c}{3} \frac{\partial}{\partial y} \left[\frac{c_B}{(K_c + c_A)^2} \frac{\partial c_A}{\partial y} \right] = D_B \frac{\partial^2 c_B}{\partial y^2} \ . \tag{14}$$

Nondimensionalizing with $\bar{c}_B = \frac{c_B}{c_{B0}}$ and the definitions in equation (7), we obtain

$$Y \frac{\partial \bar{c}_B}{\partial X} + \frac{\alpha\beta}{3} \frac{\partial}{\partial Y} \left[\frac{\bar{c}_B}{(1 + \beta \bar{c}_A)^2} \frac{\partial \bar{c}_A}{\partial Y} \right] = \delta \frac{\partial^2 \bar{c}_B}{\partial Y^2} \ , \tag{15}$$

where α, β and δ are, respectively,

$$\alpha = \frac{\chi_0}{D_A} \ , \quad \beta = \frac{c_{A0}}{K_c} \quad \text{and} \quad \delta = \frac{D_B}{D_A} \ . \tag{16}$$

These three dimensionless parameters characterize this transport problem. The representative values are $\alpha = 0.6$, $\beta = 1.4$ and $\delta = 0.35$, respectively, which correspond to the typical values of the chemotaxis parameters. We note from equation (12) that $\frac{v_{Bx}}{\dot{\gamma} y} = O(\alpha Pe^{-\frac{1}{3}}) \ll 1$ for $\alpha = O(1)$.

The boundary conditions for $\bar{c}_B$ are

$$\bar{c}_B(X, \infty) = 1 \ , \quad \bar{c}_B(0, Y) = 1 \ , \quad \frac{\alpha\beta \ \bar{c}_B}{3(1+\beta)^2} \frac{\partial \bar{c}_A}{\partial Y} - \delta \frac{\partial \bar{c}_B}{\partial Y} = 0 \quad \text{at} \quad Y = 0 \ , \tag{17}$$

which brings in the solution (10).

Then, similar to the chemoattractant case, we can seek a similarity solution $C_B(\eta) = \bar{c}_B(X, Y)$ where $\eta = \frac{Y}{(3X)^{\frac{1}{3}}}$. We find that equation (15) simplifies to an ordinary differential equation

$$-\eta^2 \frac{dC_B}{d\eta} + \frac{\alpha\beta}{3} \frac{d}{d\eta} \left[\frac{C_B}{(1 + \beta C_A)^2} \frac{dC_A}{d\eta} \right] = \delta \frac{d^2 C_B}{d\eta^2} \ , \tag{18}$$

with two boundary conditions

$$\left[\frac{\alpha\beta}{3} \frac{C_B}{(1+\beta)^2} \frac{dC_A}{d\eta} - \delta \frac{dC_B}{d\eta} \right]_{\eta=0} = 0 \quad \text{and} \quad C_B(\eta \to \infty) = 1 \ . \tag{19}$$

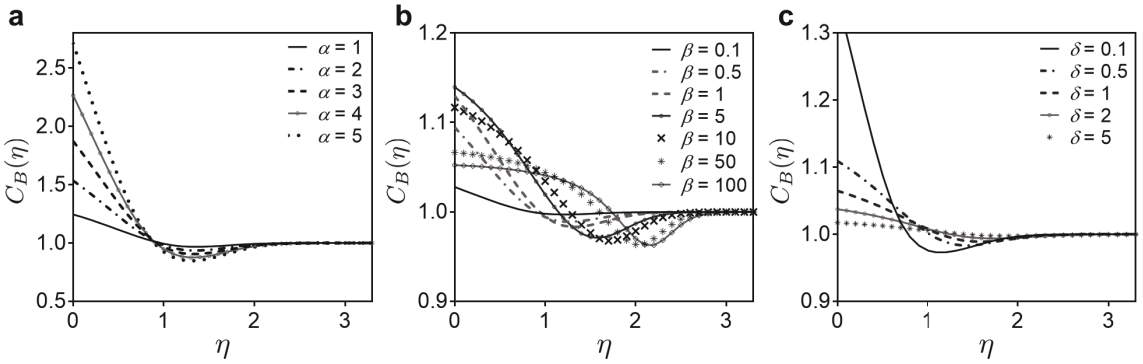

Figure 3: (a) $C_B(\eta)$ plotted versus η for (a) different values of α, (b) β, and (c) δ. (a) The values of β and δ are, respectively, 1.4 and 0.35. (b) $\alpha = 0.6$ and $\delta = 0.35$. (c) $\alpha = 0.6$ and $\beta = 1.4$. Note that the vertical scales do not extend to zero.

The transport problem involves the chemoattractant concentration profile $C_A(\eta)$ in both the equation and boundary condition at $\eta = 0$. The numerical solutions of equation (14) and (17) are plotted in Figure 2(b-c). In the vicinity of both $\eta = 0$ and $Y = 0$, we obtain accumulation of bacteria due to chemotaxis. We note that the solution is nonmonotonic as it varies between a maximum at the interface ($\eta = Y = 0$) and an asymptotic solution far away ($\eta \gg 1$). An increase in X corresponds to an increase in the exposure of the bacterial population to the chemoattractant source, thus increasing the accumulation of bacteria near the source.

We tested the effects of α, β, and δ individually in Figure 3; recall the definitions in equation (16). Both increasing α and $\beta(< O(10))$ increases the chemotactic accumulation of bacteria, while an increase in δ decreases the accumulation of bacteria at the boundary, as shown in Figures 3(a, b) and (c), respectively. We can understand these trends in terms of the physical behavior that an increase in α corresponds to an increase in the strength of the chemotactic response relative to the spread of the chemoattactant, thus concentrating the bacteria closer to the source. An increase in β corresponds to a decrease

in the concentration at which the bacteria are most sensitive to the chemoattractant, which means the bacteria are able to sense the chemoattractant over a greater distance from the source. An increase in δ corresponds to an increase in the motility of bacteria (which tends to disperse the population) compared to the spread of the chemoattractant, which will tend to reduce the accumulation near the source of chemoattractant. Also, we find

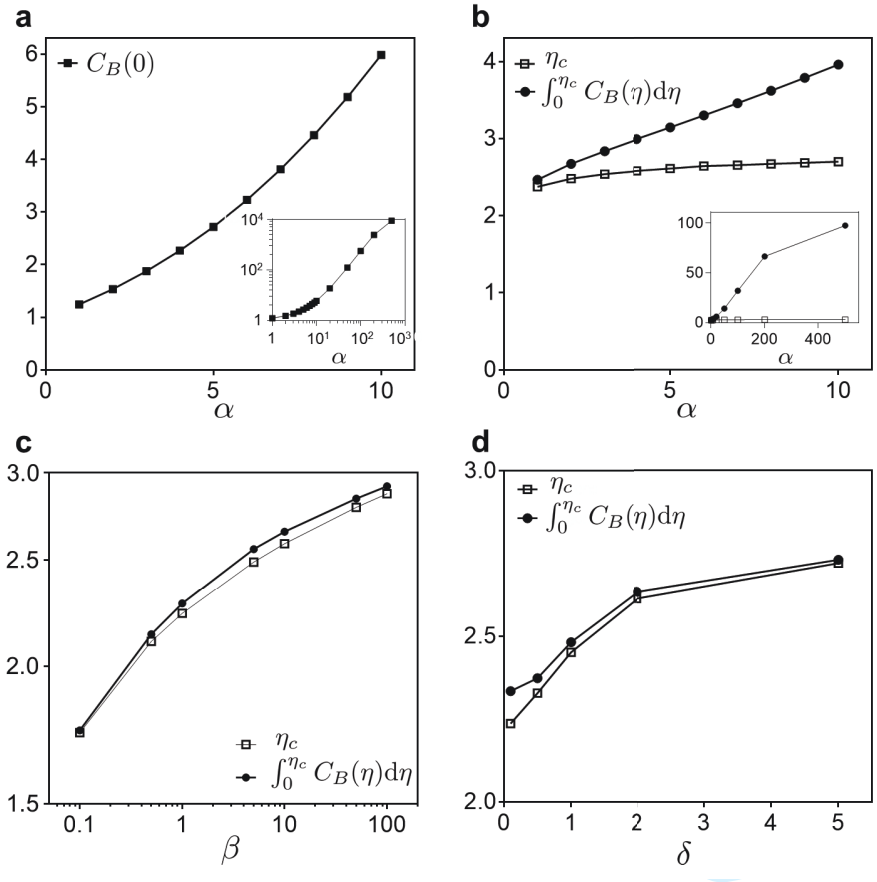

Figure 4: (a, b) Accumulation of bacteria versus α which represents the chemotactic sensitivity. Inset graphs are for larger range of α. $\beta = 1.4$ and $\delta = 0.35$. (c) Log-log plot for critical length scale η_c and the net accumulation of bacteria versus β which represents the chemotaxis receptor constant. $\alpha = 0.6$ and $\delta = 0.35$. (d) η_c and the net accumulation plotted versus δ. $\alpha = 0.6$ and $\beta = 1.4$.

that for $\beta \gtrsim O(10)$, there is accumulation at the boundary, i.e., $C_B(0)$, though it is now decreasing with β. This result shows that large (excess) concentration of chemoattractant c_{A0} compared to the chemotactic receptor constant K_c decreases the chemotaxis of bacteria near the interface.

From the similarity solutions for bacteria $C_B(\eta)$ and $\bar{c}_B(X, Y)$, we can identify a critical distance η_c or Y_c (for a given X) above which the bacterial concentration is unperturbed by chemotaxis; this distance depends on α, β and δ, as indicated in the different panels in Figure 3. We define η_c according to $C_B(\eta_c) = 0.999$ so that for $\eta > \eta_c$ the bacterial concentration is effectively not influenced by chemotaxis. We consider other features of the bacterial distribution curves to provide additional information on the effect of the dimensionless groups α, β and δ (Figure 4). For example, in Figure 4(a), we plot $C_B(0)$ versus η to understand the effect of the dimensionless chemotactic sensitivity coefficient α on accumulation of bacteria at the oil-water interface. Both for moderate values (Figure 4(a)) and over a larger range (inset) of α, the accumulation of bacteria increases monotonically as α increases. One additional observation on the effect of α is that the critical lengthscale of the region of influence η_c does not vary significantly over a larger range of α (Figure 4(b)). The net accumulation of bacteria within the region of influence ($= \int_0^{\eta_c} C_B(\eta)\mathrm{d}\eta$) is also plotted for different values of α in Figure 4(b). While the critical length scale η_c does not increase much over wide range of α, the net accumulation of bacteria within the region of influence increases with an increase of α, which is related to the increase in $C_B(0)$ at the interface.

We investigate the effect of β, which is the effect of chemoattractant concentration relative to the chemotaxis receptor constant (c_{A0}/K_c), in Figure 4(c); note the logarithmic axes. This parameter has larger impact on the values of η_c than α and tends to show a weak power-law dependence on β (the trend is almost linear in the log-log plot). The

region of influence depends on the chemoattractant concentration to which the bacteria are most sensitive chemotactically. However, an increase in β does not change the net accumulation ($\int_0^{\eta_c} C_B(\eta)\mathrm{d}\eta$) much for a large range of β because η remains close to unity. Moreover, the value of the integral is close to η_c over the investigated range of β. Figure 4(d) shows the effect of δ on the η_c and the net accumulation of bacteria within η_c. These values tend to increase for an increase in bacterial diffusivity δ. The trend shown in Figure 4(d) is consistent with our observation from Figure 3(c) that the largest change in $C_B(0)$ is observed for $\delta \lesssim 1$.

In experimental systems, the effect of α and β are coupled, which complicates the analysis for individual parameters [11]. The model described here suggests better understanding of important factors on the chemotatic accumulation of bacteria at the oil-water interface under shear flow by showing different dependency on α, β and δ. This means that we can use different features of the experimental observations to determine values for these two parameters.

Finally, from the definition of similarity variable η, we can simply write the relation

$$y_c = \eta_c \left(3x(D_A/\dot{\gamma})\right)^{\frac{1}{3}}, \tag{20}$$

and learn the effect of shear rate on the region of chemotaxis. To get a sense of the dimensional scale of the region, we plot y_c versus x in Figure 5(a) for typical values $D_A = 8.6 \times 10^{-10}$ m^2/s and $\dot{\gamma} = 30$ s^{-1}. For $\alpha = 0.6$, $\beta = 1.4$ and $\delta = 0.35$, the critical similarity variable $\eta_c = 2.29$. The inset of Figure 5(a) shows the trend of y_c at $x = 50$ μm versus shear rate. This value should not be directly compared to the actual length measured from experiments as our calculations have many approximations, but η_c as a function of shear rate can provide physical insight (e.g. proper choice of measurement windows) for experimental studies of chemotaxis in similar configurations.

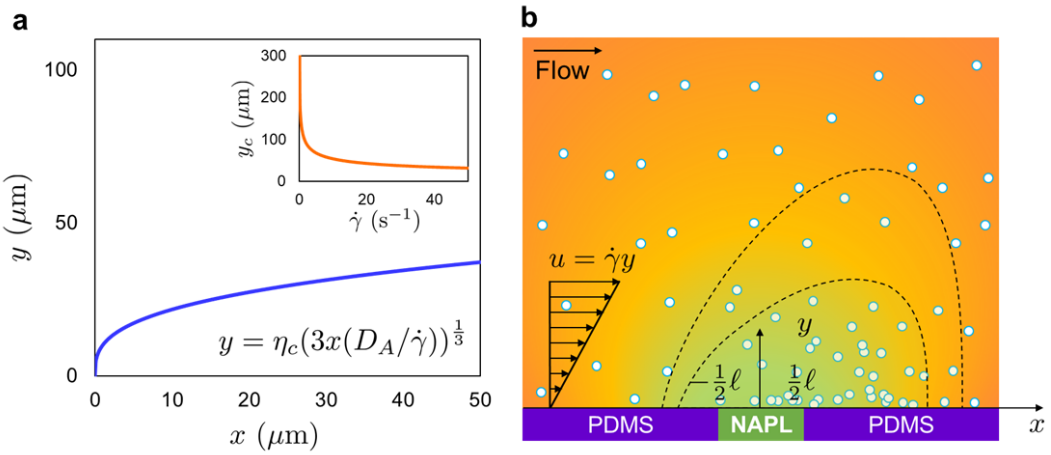

Figure 5: (a) The region of influence y is plotted versus x for $\eta_c = 2.29$, $D_A = 8.6 \times 10^{-10}$ m^2/s and $\dot{\gamma} = 30$ s^{-1}. Inset: critical length scale y_c at a fixed position $x = 50$ μm is plotted versus shear rate $\dot{\gamma}$. (b) Schematic suggesting possible shape of region of influence as "chemotaxis contours" for the geometry used in [6].

Throughout the paper we studied the fast flow limit (Pe $\gg 1$) with a simplified geometry where there is no fixed geometric length scale. Detailed investigation for the more general problem with the geometry described in Figure 1(b) will suggest chemotaxis contours (dotted lines in Figure 5(b)), which are the curves that enclose the region of chemotactic influence (bacterial accumulation) under certain flow conditions. This remains as future work.

III. Conclusion

We solved a two-dimensional, steady-state model for bacterial chemotaxis when the chemoattractant diffuses into an aqueous phase in the transverse direction to the flow. We applied a shear flow approximation near the interface between NAPL and the aqueous phase and identified a similarity variable. Similarity solutions for the concentration of chemoattrac-

tant and bacterial distribution demonstrate effects of important parameters such as the chemotatic sensitivity, the chemotaxis receptor constant, and the motility of bacteria. Moreover, the similarity solutions suggest a critical length scale η_c for the region of chemotaxis. From the definition of η and the "boundary layer" nature of the region of bacterial accumulation, we further suggest contours of chemotaxis and selection of appropriate observation windows. A more detailed model is necessary for lower Peclet numbers or more complicated geometries. However our calculations provide important insight to the system by investigating the nondimensional groups separately and by identifying a typical length scale for chemotaxis near a chemoattractant source exposed to flow.

Acknowledgements

We thank Bhargav Rallabandi for useful discussions on the conservative feature of the finite-volume method. This research was made possible in part by a grant from The Gulf of Mexico Research Initiative, and in part by NSF via CBET-1702693. Data are publicly available through the Gulf of Mexico Research Initiative Information & Data Cooperative (GRIIDC) at https://data.gulfresearchinitiative.org.

References

[1] Mackay DM, Cherry JA. Groundwater contamination: pump-and-treat remediation. Environ. Sci. Technol. 1989;23:630-636

[2] Pandey G, Jain RK. Bacterial chemotaxis toward environmental pollutants: role in bioremediation. Appl. Environ. Microbiol. 2007;109:1622-1628

[3] Parales RE, Ditty JL, Harwood CS. Toluene-degrading bacteria are chemotactic towards the environmental pollutants benzene, toluene, and trichloroethylene. Appl. Environ. Microbiol. 2000;66:4098-4104

[4] Law AMJ, Aitken MD. Bacterial chemotaxis to naphthalene desorbing from a nonaqueous liquid. Appl. Environ. Microb. 2003;69:5968-5973

[5] Ford RM, Harvey RW. Role of chemotaxis in the transport of bacteria through saturated porous media. Adv. Water Resour. 2007;30:1608-1617

[6] Wang X, Long T, Ford RM. Bacterial chemotaxis toward a NAPL source within a pore-scale microfluidic chamber. Biotechnology and Bioengineering. 2012;109:1622

[7] Lanning LM, Ford RM, Long T. Bacterial chemotaxis transverse to axial flow in a microfluidic channel. Biotechnology and bioengineering. 2008;100:653-663

[8] Ahmed T, Shimizu TS, Stocker R. Bacterial chemotaxis in linear and nonlinear steady microfluidic gradients. Nano Letters. 2010;10:3379-3385

[9] Ahmed T, Shimizu TS, Stocker R. Microfluidics for bacterial chemotaxis. Integr. Biol. 2010;2:604-629

[10] Wolfram CJ, Rubloff GW, Luo X. Perspectives in flow-based microfluidic gradient generators for characterizing bacterial chemotaxis. Biomicrofluidics. 2016;10:061301

[11] Wang X, Atencia J, Ford RM. Quantitative analysis of chemotaxis towards toluene by *Pseudomonas putida* in a convection free microfluidic device. Biotechnol. Bioeng. 2015;112:896-904

[12] Long T, Ford RM. Enhanced transverse migration of bacteria by chemotaxis in a porous T-sensor. Environ. Sci. Technol. 2009;43:1546-1552

[13] Locsei JT, Pedley TJ. Run and tumble chemotaxis in a shear flow: the effect of temporal comparisons, persistence, rotational diffusion and cell shape. Bull. of Math. Biol. 2009;71:1089-1116

[14] Chen KC, Ford RM, Cummings PT. Perturbation expansion of Alt's cell balance equations reduces to Segel's one-dimensional equations for shallow chemoattractant gradients, Siam J. Appl. Math. 1998;59:35-57

[15] Duffy KJ, Ford RM, Turn angle and run time distributions characterize swimming behavior for *Pseudomonas putida*, J. Bacteriol. 1997;179:1428-1430

[16] Stone HA, Stroock AD, Ajdari A. Engineering flows in small devices: Microfluidics toward a lab-on-a-chip, Ann. Rev. Fluid Mech. 2004;36:381-411

[17] Squires TM, Quake SR. Microfluidics: Fluid physics at the nanoliter scale, Review of Modern Physics. 2005;77:977-1026

[18] Purcell EM, Life at low Reynolds number, Am. J. Phys. 1977;45:3-11

[19] Molaei M, Sheng J, Succeed escape: Flow shear promotes tumbling of *Escherichia coli* near a solid surface. Sci. Rep. 2016;6:35290

[20] Molaei M. Barry M, Stocker R, Sheng J, Failed escape: Solid surfaces prevent tumbling of *Escherichia coli*. Phys. Rev. Lett. 2014;113:068103

[21] Kaya T, Koser H. Direct upstream motility in *Escherichia coli*, Biophys. J. 2012;102:1514-1523

[22] Lauga E, Bacterial hydrodynamics, Annu. Rev. Fluid Mech. 2016;48:105-130

[23] Deen WM. Analysis of Transport Phenomena. Oxford University Press, 1998

[24] Ristenpart WD, Stone HA. Michaelis-Menten kinetics in shear flow: Similarity solutions for multi-step reactions, Biomicrofluidics. 2012;6:014108

< **Revisions made to the article 2** >

Chemotaxis in shear flow: similarity solutions of the steadystate chemoattractant and bacterial distributions

Suin Shim[1], **Howard A. Stone**[1] **and Roseanne M. Ford**[2,*]

[1]*Department of Mechanical and Aerospace Engineering, Princeton University, Princeton, NJ 08544, USA*

[2]*Department of Chemical Engineering, University of Virginia, Charlottesville, VA 22904, USA*

Page 3

Figure 1(c) and the caption of Figure 1 are revised.

(a) Experimental image from Wang et al. [6]. The white dots in the background are bacterial cells. Scale bar is 100 μm. (b) Schematic drawing for arbitrary Peclet number of the flow near the chemoattractant window as an approximation to the shear flow near a surface. Bacterial suspension is indicated as white dots and the green and orange colors approximates the chemoattractant distribution. We solve for the chemoattractant and bacterial concentration in the aqueous phase. For the general problem statement, we consider the region that is larger than the typical length scale of the oil-water interface. (c) Schematic of the shear flow near the chemoattractant for the large Peclet number limit ($Pe \gg 1$). In this limit, we analyze the boundary region near the downstream part of the NAPL entrance and we shift the origin of the x axis.

Page 5

Typical swimming speed of P. putida is added: (≈ 44 μm/s for *P. putida* [15])

Page 6 *After the equation (4c), revised sentences:* where $D_B = 3.2 \times 10^{-10}$ m^2/s is a representative value from the experimental system [6]. We note that the parameter value for bacterial diffusion is based on cell motility in a bulk aqueous phase.

At the end of the page: In some cases, bacteria in shear flow near surfaces tend to swim upstream along the surface [21,22] though this is an effect we neglect below because our interest is on transport of bacteria from the bulk fluid to the interface rather than over the interface.

Page 14,15 Figure 5(a) is replotted for $\dot{\gamma} = 30$ s^{-1} and the corresponding caption and text ($\dot{\gamma} = 30$ s^{-1}) are changed.

References added

[21] Kaya T, Koser H. Direct upstream motility in *Escherichia coli*, Biophys. J. 2012;102:1514-1523

[22] Lauga E, Bacterial hydrodynamics, Annu. Rev. Fluid Mech. 2016;48:105-130